DEVELOPMENT OF CHILD PEDESTRIAN MATHEMATICAL MODELS AND EVALUATION WITH ACCIDENT RECONSTRUCTIONS

Xuejun Liu and Jikuang Yang
Crash Safety Division, Department of Machine and Vehicle Design
Chalmers University of Technology, Göteborg, Sweden

ABSTRACT

Four mathematical models representing 3-, 6-, 9- and 15-year-old children were developed based on a validated mathematical model of adult pedestrian. The basic anthropometric data of these child models were generated by GEBOD program according to the age and body height/weight. Due to the absence of biomechanical data of children, scaling methods were applied to derive the stiffnesses of joints and the contact properties of body segments from that used in the validated adult model. Differences in anatomy structures between adults and children, as well as age-dependent properties of bone and ligament, were incorporated into these child models. In the present study, the main efforts were focused on the scaling of neck, thoracic, lumbar and knee joint properties, as well as the contact stiffnesses of the lower extremities.

To evaluate the validity of these child pedestrian models, two real-world child accidents were reconstructed by using the accident data from in-depth case studies. The dynamic responses of the mathematical models agreed reasonably well with the injury outcomes in accidents.

KEYWORDS Children, Pedestrians, Scaling, Accident Reconstructions

CHILD PEDESTRIAN ACCIDENTS are one of the major causes of child casualties and disabilities. Even though the importance of child pedestrian protection has been recognized for almost three decades (Ashton et al., 1974), there is still very limited progress in the research on child pedestrian injuries. Up until now, no mechanical dummy or mathematical model has been specifically developed to represent child pedestrians.

Analysis of child pedestrian accidents indicated that, all age groups of children up to 14 years are almost equally exposed (Pitt et al., 1990), and body height plays an important role in injury patterns (Ashton, 1979). Younger children (<6) are more likely to be killed than elder children (>9) because of the impact between the stiff hood edge and head, while elder children sustain severe head injuries as a result of the contact between head and front part of hood top (Sturtz et al., 1976; Ohashi, 1990). Besides the most frequent skull-brain trauma, child pedestrian victims are often subjected to the fractures of the lower extremities and the injuries to internal organs of the abdomen (Sturtz et al., 1976). The majority, more than 80% of the child pedestrians, are hit from the side by a vehicle fronts. This primary impact leads to more severe injuries than that secondary impact against ground (Sturtz et al., 1976; Ashton, 1979; Ohashi, 1990).

To evaluate the injury severities of children under certain impact loading, the biomechanical knowledge of children are desirable. However, only 8 child occupant impact tests had been performed with cadaver specimens (Brun-Cassan et al., 1993). Due to the remarkable variations between these children subjects, as well as the different loading condition between occupant and pedestrian, the results obtained from these experiments should be interpreted with great caution.

Therefore, scaling method has been widely accepted and applied to develop the dummies of infant (Melvin, 1995), child occupant (Irwin and Mertz, 1997), small female and large male adult (Mertz et al., 1989). One general principle of the scaling process was based on the normalizing impact response

data (Mertz, 1984), which assumed that the impact responses can be represented by a simple spring-mass system. Another technique is to use the dimensional analysis (Melvin, 1995) based on the fact that all engineering units can be divided into mass, time, and length. Some studies incorporated the material properties by multiplying the ratio of elastic moduli of bone with the dimensional scaling factor, regardless of the developing anatomy structures of children (Irwin and Mertz, 1997; Melvin, 1995). A more realistic scaling approach by Yoganandan et al. (2000) was based on the accurate description of neck structures with Finite Element Method (FEM). Both effects of anatomy structures and material properties were accommodated. Nevertheless, none of the studies mentioned above dealt with the scaling method for the development of child pedestrian models.

The objective of this study is to develop the mathematical models of child pedestrians up to 15 years old, and evaluate the validity of these child models by means of the reconstructions of real-world accidents.

MATERIAL AND METHODS

As a basis of the present study, Yang et al. (2000) developed a series of human-like pedestrian models representing adults with different sizes. These models were validated against full-scale impact tests with cadavers. The anthropometric data for the models were generated by GEBOD program (TNO, 1999). The characteristics of the body segments and the joints were defined based on available biomechanical data from literature.

In this study, the sophisticated simulation package MADYMO (TNO, 1999) was applied to build up the basic configuration of the models including the mass, inertial properties, sizes of the body segments, as well as the joint locations. The characteristics of the joints, contact stiffness of the body segments, were scaled down from the validated 50th percentile male adult model (Yang et al., 2000).

The scaling factors used in this study were derived from existing biomechanical data, anatomy structures and age-dependent properties of the soft tissues and bones. Since most of the child pedestrians are struck from the side, the model set-up focuses on the lateral properties of neck, thoracic, lumbar and knee joints. The contact stiffnesses of critical parts (head, thorax and lower extremities) were also scaled.

The validity of the child models was examined with reconstructions of two real world accidents. The dynamic responses of the child models were compared with the head injury outcomes registered in police and medical reports. Moreover, the rest positions and throw out distances of child pedestrians were also correlated to that recorded at accident scenes.

CONFIGURATION OF CHILD PEDESTRIAN MODELS - Each model consists of fifteen ellipsoids connected by 14 joints. The body segments include the head, neck, thorax, abdomen, pelvis, left/right upper arm, left/right forearm, left/right thigh, left/right leg, and left/right foot. In order to simulate the lateral flexion, all the joints are defined as the 3-dimensional spherical joint, which allows the rotational but no translation movement between two connected ellipsoids. A comparison of body sizes among the child models at 3-, 6-, 9-, 15-year-old (hereafter referred as 3YOC, 6YOC, 9YOC and 15YOC respectively) and 50% adult male model were give in Fig. 1.

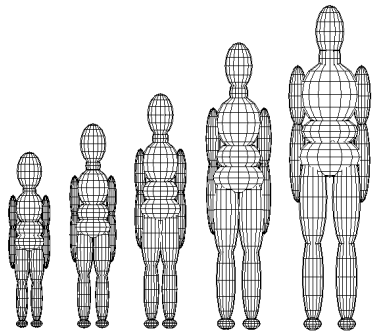

Fig. 1 - Configurations of child pedestrian models at 3, 6, 9 and 15 years old, compared with 50% adult male model (from left to right)

Characteristic dimensions of the children were summarized in Table 1, along with those for the 50% adult male. These anthropometric dimensions were consistent with that for Hybrid III child dummies (Irwin and Mertz, 1997). The total body weight, mass distribution and inertial property of each child model were also obtained directly from the GEBOD program.

Table 1. Characteristic dimensions of child pedestrians and the 50% adult male

Body Dimensions (mm)	3YOC	6YOC	9YOC	15YOC	Adult
Standing Height	989	1150	1310	1631	1780
Shoulder Height	769	907	1046	1324	1458
Head Depth	178	181	185	191	199
Head Width	136	139	143	149	156
Head to Chin Height	175	184	192	208	228
Neck Circumference	235	256	277	318	384
Chest Depth	159	185	211	264	246
Chest Width	156	181	206	255	328
Hip Width, Standing	173	206	238	303	354
Forearm-hand Length	259	304	348	438	496
Biceps Circumference	151	175	200	248	316
Forearm Circumference	152	172	193	235	282
Knee Height, Seated	298	352	406	514	560
Thigh Circumference	292	347	402	514	589
Upper Leg Circumference	247	291	335	423	388
Knee Circumference	247	291	335	423	394
Calf Circumference	202	234	267	332	373
Ankle Circumference	146	162	179	211	225
Body Weight (kg)	10.5	21.3	32.1	53.8	79.3

Based on these characteristic measurements of children and adult, dimensional scale factors λ in x-, y-, and z-direction for various body segments can be derived. For example, Head depth, head width and head to chin height were selected to derive the dimensional scale factors λ_x, λ_y, λ_z, respectively. Neck circumference was chosen to calculate the scale factors λ_x, λ_y, while the scale factor in z-direction (λ_z) of neck was estimated from total body height, shoulder height, and head to chin height. Similarly, other important dimensional factors were calculated, as given in Table 2.

Table 2. Dimensional scale factors for 3-, 6-, 9- and 15-Year-Old child with respect to the 50th percentile adult male

Dimensional Scale Factors	3YOC			6YOC			9YOC			15YOC		
	λ_x	λ_y	λ_z	λ_x	λ_y	λ_z	λ_x	λ_y	λ_z	λ_x	λ_y	λ_z
Pelvis	0.46	0.50	0.60	0.66	0.58	0.68	0.77	0.67	0.77	0.90	0.86	0.95
Lumber Spine	0.47	0.38	0.60	0.66	0.54	0.68	0.78	0.63	0.77	0.92	0.74	0.95
Abdomen	0.50	0.43	0.60	0.63	0.58	0.68	0.70	0.67	0.77	0.75	0.78	0.95
Thoracic Spine	0.65	0.48	0.60	0.75	0.55	0.68	0.86	0.63	0.77	0.91	0.77	0.95
Neck	0.61		0.60	0.67		0.68	0.72		0.77	0.83		0.95
Head	0.85	0.93	0.78	0.87	0.95	0.81	0.88	0.98	0.85	0.92	1.02	0.92
Upper Arm	0.48		0.56	0.55		0.67	0.63		0.78	0.79		1.01
Lower Arm	0.54		0.54	0.61		0.65	0.68		0.75	0.83		0.96
Hand	0.44		0.56	0.61		0.66	0.72		0.76	0.83		0.96
Upper Leg	0.48		0.52	0.69		0.65	0.81		0.78	0.96		1.04
Lower Leg	0.63		0.58	0.74		0.68	0.85		0.78	1.07		0.97
Feet	0.45	0.52	0.58	0.62	0.71	0.68	0.72	0.81	0.78	0.81	0.91	0.97

EXISTING BIOMECHANICAL DATA - Very little biomechanical data can be found directly from the available child cadaver tests. Mcpherson and Kriewall (1978) studied the elastic moduli for the bending of the parietal bones of two full-term newborns (2.5 GPa) and one 6-year-old child (6.6 GPa). Hubbard and Soutas-Little (1984) reported an elastic bending modulus 9.9 GPa for the adult parietal bone. Based on the results above, a cubic spline fit (Fig. 2a) was performed to estimate the elastic moduli for the parietal bone for other ages (Irwin and Mertz, 1997).

The mechanical property of ligament varies significantly with ages (Beusenberg et al., 1993), and is strongly connected to the characteristics of joints (Kapandji, 1970). The force-elongation properties of ligaments for 1-, 3-, 6-, and 11-year-old children were gathered by Kumaresan et al. (1997) and Yoganandan et al. (2000). The scale factors of ligament properties were calculated (Fig. 2b), of which the factors for 9- and 15-year-old child were estimated from a cubic spline fit to these data.

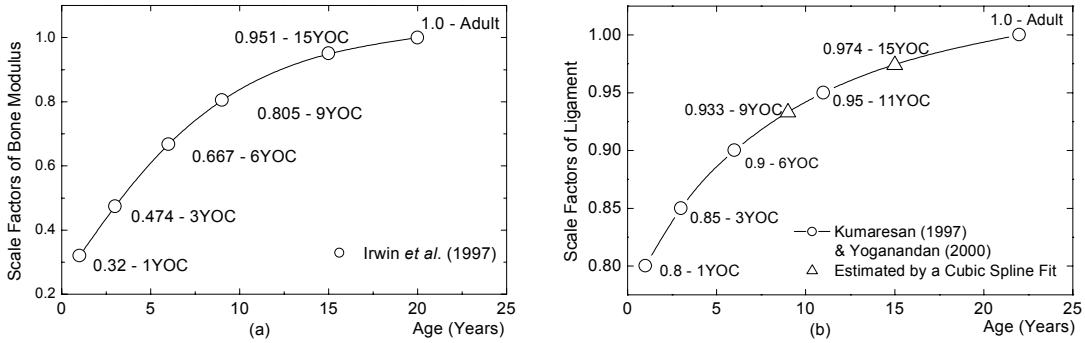

Fig. 2 - Scale factors of (a) elastic modulus of parietal bone (Irwin and Mertz, 1997), (b) ligament stiffness (Kumaresan et al., 1997; Yoganandan et al., 2000)

SCALING OF JOINTS PROPERTIES - For the pedestrian involved in a car accident, the lateral flexion properties are significant for the dynamic responses of the whole human body (Yang, 1997). The lateral flexion property of the entire spinal column is mainly controlled by the strength of soft tissues connecting vertebrae.

In the child pedestrian models, the entire vertebra column was simulated by four spherical joints, including upper and lower neck, thoracic as well as lumbar joints. To scale the stiffnesses of these joints, it is advisable to begin the analysis of resistive mechanism with a function unit. In this study, the function unit of the entire vertebra column was demonstrated with two vertebral plateaus in lumbar vertebra (Fig. 3a), which are connected by the contralateral intertransverse ligament (1) and the ipsilateral ligaments (2) (Kapandji, 1970). During lateral flexion, the body of upper vertebra tilts ipsilaterally. This leads to the elongation of the contralateral intertransverse ligament (1), whereas the ipsilateral ligament (2) relaxes. The articular processes slide relative to each other so that the ipsilateral process of the upper vertebra is raised (3), while the contralateral process is lowered (4). Within the range of physiological movement, the resultant moment of intertransverse ligament balances the external lateral impact loading.

Similar resistive mechanism can be used to describe the lateral bending stiffness of knee joints (Fig. 3b) . This is a common injury mechanism of the knee joints in car to pedestrian impacts (Yang and Kajzer, 1992). In this model, the medial collateral ligament provides the main resistant force against external impact force.

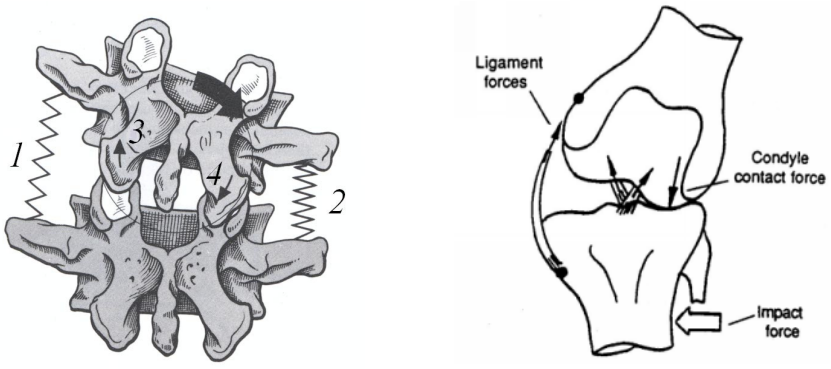

(a) (b)

Fig. 3 – Analysis of anatomic structures (a) the posterior view of the functional unit in lumbar vertebra (adopted from Kapandji, 1970), (b) the resistive mechanism of knee joint under lateral impact loading (Yang and Kajzer, 1992)

For simplicity and clarity reason, a theoretical model of lateral flexion mechanism was built up with an example of the knee joint, which is also applicable to the cervical, thoracic, lumbar as well as ankle joints (Fig. 4).

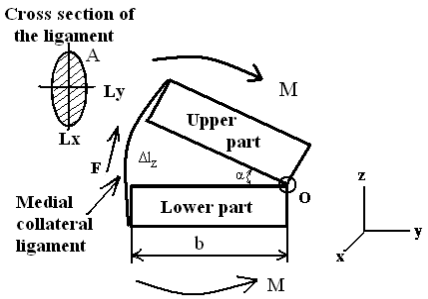

Fig. 4 - Simplified resistive mechanism of knee joint in lateral flexion loading

The medial collateral ligament provides the resistive moment of knee lateral bending, which can be expressed as:

$M=F\times b$ (1)

where M is the resistive moment of knee joint, F the resultant force of medial collateral ligament, b the effective moment arm of knee joint.

Mechanically the resultant force of medial collateral ligament can be expressed as:

$F=\sigma\times A$ (2)

where σ is the effective stress of medial collateral ligament, A is the sum of the cross sectional area of the medial collateral ligament.

Combining equation (1) and (2) gives,

$$M=\sigma Ab=E\varepsilon Ab=E\frac{\Delta l_z}{l_z}\pi l_x l_y b=E\frac{b\times\alpha}{l_z}\pi l_x l_y b=E\pi\frac{b^2 l_x l_y}{l_z}\alpha \quad (3)$$

where E is the elastic modulus of ligament tissue, l_x, l_y, l_z are the depth, width and length of the medial collateral ligament respectively. The cross sectional area of the medial collateral ligament was assumed as ellipsoid with the area of $A=\pi\times l_x\times l_y$. The lateral bending angle of knee is denoted as α.

Therefore the lateral bending stiffness of knee joint can be expressed as:

$$k_{lateral\,bending}=\frac{M}{\alpha}=E\frac{b^2 l_x l_y}{l_z}\pi \quad (4)$$

This indicated that the lateral bending stiffness of knee joints depends on depth, width, length and the elastic modulus of medial collateral ligament, as well as the width of the tibia condyle. However, limited anatomic measurement data of bones and soft tissues is available for children at different age, an assumption had to be made in this study.

Assuming that the width of tibia condyle, b, is proportional to the width of lower leg while the length l_z, width l_y and depth l_x of the media collateral ligament are proportional to the length of tibia, width of tibia, and depth of tibia, respectively. The ratio of the ligament E modulus between child and adult is λ_E, the ratio of tibia depth is λ_x, the ration of tibia width is λ_y, and the ratio of the whole length of femur and tibia is λ_z. The scaling factor of lateral bending stiffness between child and adult can be expressed as,

$$\lambda_k=\lambda_E\frac{\lambda_x\lambda_y^3}{\lambda_z} \quad (5)$$

This scaling method can also be applied to the vertebrae column. For example in neck joint, the λ_x, λ_y and λ_z refer to the scale factors in the depth, width and length of neck (Table 2), while λ_E is the scale factor for ligaments (Fig. 2b). The scale factors of thoracic and lumbar joints can be derived in the similar way.

The hip joint stiffness was not scaled based on the anatomic point of view, but the relationship in equation (5) was applied to hip joint at current stage of this study. All these scale factors for the lateral flexion properties of various joints were listed in Table 3.

Table 3. Scale factors for the lateral flexion properties of joints

Scale factors	Age			
	3YOC	6YOC	9YOC	15YOC
Neck Joint	0.20 (0.18*)	0.27(0.24*)	0.33	0.49
Thoracic Joint	0.10	0.17	0.26	0.43
Lumbar Joint	0.04	0.14	0.24	0.38
Knee Joint	0.23	0.40	0.62	1.31
Ankle Joint	0.09	0.29	0.46	0.61
Shoulder Joint	0.08	0.12	0.19	0.38
Hip Joint	0.09	0.31	0.51	0.80
Elbow Joint	0.13	0.19	0.27	0.48

* Results of Yoganandan et al. (2000)

SCALING OF CONTACT STIFFNESSES - Another aspect of developing the child pedestrian model is to scale the contact stiffnesses of various body segments. For long bones like the tibia and femur, the contact stiffness can be described with the force (F) and deflection (δ) relationship in a three-point bending mode (Fig. 5).

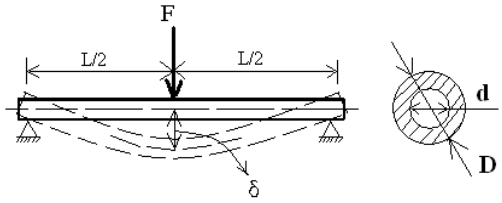

Fig. 5 - Three-point bending mode of long bones

The cross section of the bone was assumed as a cylinder with outer diameter of D and inner diameter of d. Under central loading of F, the deflection δ follows the relationship:

$$\delta = \frac{FL^3}{48EI} \tag{6}$$

where L is the length of bone, E is the E-modulus, I is the cross-section moment expressed as:

$$I = \frac{\pi \cdot (D-d)^4}{64} \tag{7}$$

Thus, combing equation (6) and (7) leads to the stiffness of long bone:

$$\frac{F}{\delta} \sim \frac{(D-d)^4 \cdot E}{L^3} \tag{8}$$

Since insufficient bone geometry data of outer (D) and inner diameters (d), it was assumed that $D=2d$ for the children under 15 years old (Frank, 1987). Therefore the stiffness ratio of the long bone between child and adult is given as,

$$\lambda_{stiffness} = \lambda_E \times \frac{\lambda_D^4}{\lambda_L^3} \tag{9}$$

For the long bones, the ratio λ_L equals λ_z, whereas λ_D can be estimated from the circumference of the corresponding body segments. For example, λ_L of tibia represents ratio of the length from knee joint to ankle joint, while λ_D is the ratio of calf circumference. In Table 2, λ_D was given as λ_x and λ_y.

Hence the ratio of contact stiffness of long bones can be more clearly presented as,

$$\lambda_{stiffness} = \lambda_E \times \frac{\lambda_x^4}{\lambda_z^3} \tag{10}$$

where λ_E is the ratio of bone elastic modulus (Fig. 2a).

Besides the long bones described above, the thorax is also frequently injured by vehicle frontal structure. Hamilton et al. (1988) discussed the scaling factor of thoracic lateral stiffness from adult to six years old child with Finite Element simulation. Scaling factors for thorax stiffness of 3-, 6-, 9- and 12-year-old child were proposed.

The contact stiffness of pelvis was rarely scaled in previous research studies. In this study, the scale factors for the thorax area were applied to derive the pelvis stiffness for the children at different ages.

For the scaling of head contact stiffness, Irwin and Mertz (1997) extended the scaling method of adult head responses to children. It was found that the high bulk modulus of the brain is more dominant than the elastic bending modulus of the skull. However, limited biomechanical data of children brain characteristics has been reported. It is therefore impractical to analyze the head contact stiffness from the point of view on the mechanical properties of brain and head anatomic structure. At current stage of this study, the equation (10) was adopted to derive the scale factors of head contact stiffness for the child pedestrian models.

The scale factors of contact stiffnesses of different body segments with respect to the 50th percentile adult male were summarized in Table 4.

Table 4. Scaling factors of contact stiffness of different body segments

	3YOC	6YOC	9YOC	15YOC
Tibia/Fibular	0.38	0.64	0.89	1.37
Femur	0.18	0.55	0.73	0.72
Upper Arm	0.14	0.20	0.27	0.36
Lower Arm	0.26	0.34	0.41	0.51
Thorax*	0.34	0.40	0.45	0.51
Pelvis	0.34	0.40	0.45	0.51
Head	0.63	0.86	0.98	1.08

* Results of Hamilton et al. (1988)

RECONSTRUCTIONS OF CHILD PEDESTRIAN ACCIDENTS

CASE 1: 7-YEAR-OLD CHILD AGAINST OPEL - An OPEL REKORD Caravan struck a 7-year-old (7YOC) on a secondary rural road. The driver claimed that he saw a group of children playing on the right side of the road from about 50 meters away (Position A in Fig. 6). Then he began to brake slightly as the car approaching the cross. Suddenly the 7-year-old boy began running across the street when the car arrived at position B. The driver braked hardly and turned left to avoid the child. However, the child was still hit by the right front corner of the vehicle at position C. The car stopped about 10 meters away, and threw the child to position D.

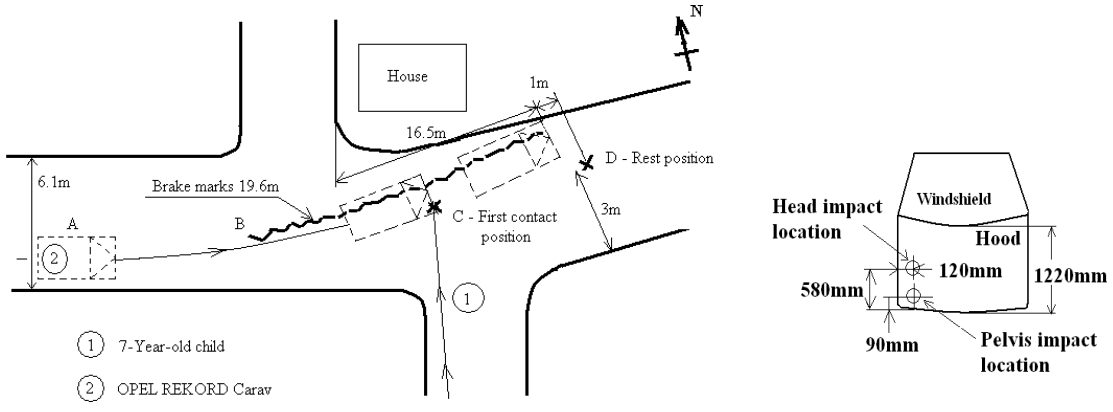

(a) (b)

Fig. 6 – Scheme drawing of (a) accident scene, (b) head and pelvis impact location on hood top

The accident car suffered slight damage. The right headlight was broken, and repaired before the inspection. Two dents were found on the hood (Fig. 6b). One was about 580 mm away from hood edge and 120mm away from right fender. It was identified as the result of child head impact. Another dent caused by the pelvis impact, was about 90mm away from the hood leading edge. No evidence indicated the damage to the structures beneath the hood.

According to the medical reports, the child was unconsciousness due to the severe brain injuries, and regained its consciousness after 13 days medical treatment in hospital. Except for some slight outer skin injuries in the lower extremities, no other injuries were reported.

A mathematical vehicle model was developed based on the schematic drawing of OPEL REKORD Caravan. The vehicle front structures were presented by four ellipsoids including lower bumper, bumper, hood edge and hood top as well. Several planes and ellipsoids were assigned to describe the outer surface and wheels. The force-deformation properties of the front structures were obtained from the sub-system test results of Euro-NCAP. The friction coefficient between the wheels and road surface was assumed to be 0.7. The diving angle was assumed as 3 degree. Steering effect was also simulated by defining an angular velocity of 1 rad/sec^2 about z-axis.

A 7-year-old child was scaled down from the validated adult model by using the scaling method described previously. The initial posture was adjusted to be running. The friction coefficient between child body segments and road surface was based on empirical data, and was set at 0.6.

CASE 2: 9-YEAR-OLD CHILD AGAINST VOLVO 850 - A 9-year-old (9YOC) child was hit by a Volvo 850 car at a crosswalk in a residential area. The accident scene was described in Fig. 7(a). The braking distance after initial impact with the child was about 7–7.5 m, and the throw-out distance of the child was around 1.5-2m. The wiper for the front right head lamp was damaged by collision. On the hood, a very slight dent was found at 630mm away from the front end and 430mm inside of the right fence Fig. 7(b). The child sustained severe brain injuries but without skull fracture. No severe injuries were found in other body areas.

The car model was configured according to the front shape of Volvo 850 car. Mechanical properties of front structures were from EURO-NCAP subsystem tests with Volvo S70. The braking deceleration was chosen as 0.7g, while the diving angle was assumed as 2 degree.

The child model was developed with the scaling method mentioned above. The initial posture was adjusted as running cross the street. The injury parameters for the head, chest, pelvis and lower extremities were calculated to evaluate the injury risks for the child.

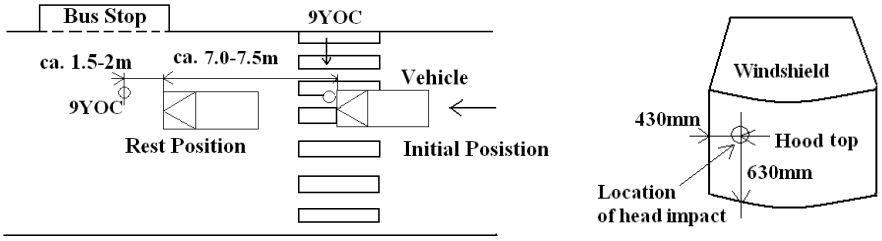

(a) (b)

Fig. 7 - Scheme drawing of (a) accident scene of 9-year-old child (9YOC) against Volvo 850, (b) head impact location on the hood top

RESULTS

7-YEAR-OLD CHILD AGAINST OPEL - The estimated vehicle travel speed was about 65-70 km/h at the initial position (Fig. 6a), and around 40 km/h at the impact position. The simulated braking distance from the cross to the vehicle rest position (Fig. 8) was about 16.1m (accident: 16.5 m), and the child throw-out distance was around 1.2 m (accident: 1 m). Both were close to the information collected by police (Fig. 6a).

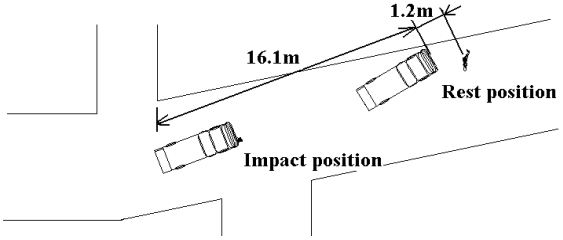

Fig. 8 – Overall trajectory of OPEL and 7-year-old child

Head impact occurs at around 60 ms after the initial contact (Fig. 9). The head impact location is 570mm (accident: 580 mm) away from hood leading edge and 120 mm (accident: 120 mm) away from right fender. The calculated injury parameters of other body segments were given in Table 5.

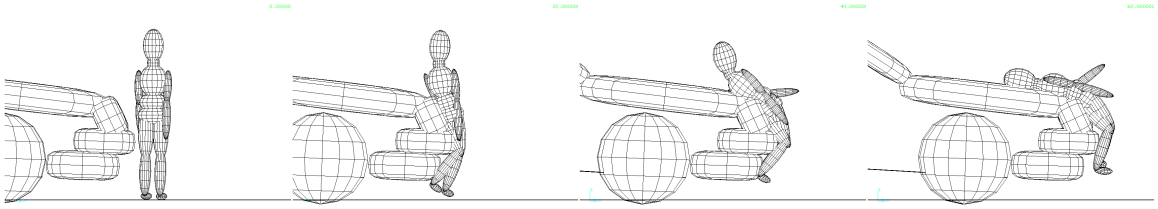

Fig. 9 - Kinematics of 7YOC and the head impact location on hood top (0-60 ms, Δt=20 ms)

9-YEAR-OLD CHILD AGAINST VOLVO 850 – After several trial simulations, the vehicle impact speed was determined as 36 km/h. The simulated braking distance (Fig. 10) after initial impact was around 7.1 m (accident: 7.0-7.5 m), and the throw-out distance of the child was reconstructed as about 1.8 m (accident: 1.5 – 2 m). The overall trajectory agreed well with the police report (Fig. 7a).

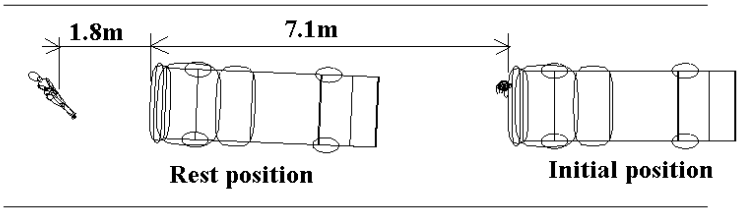

Fig. 10 - Overall trajectory of 9-year-old child and Volvo 850

The head impact happened at around 85 ms after the initial impact between the child and the accident car (Fig. 11). The impact location was about 620 mm (accident: 630 mm) from the hood leading edge, and 430 mm (accident: 430 mm) from the right fender, which matched well with the inspection result of the accident car (Fig. 7b).

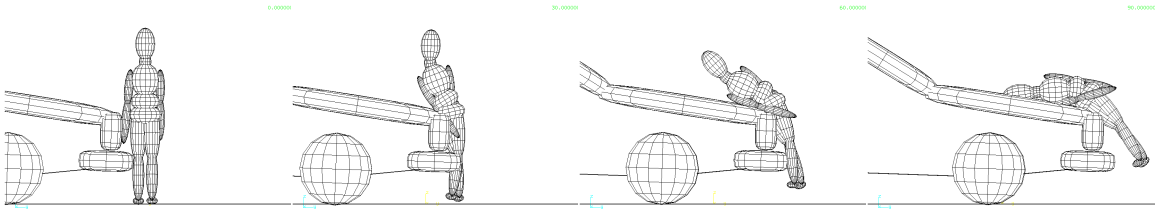

Fig. 11 - kinematics of 9YOC and head impact location on the hood top (0-90 ms, Δt=30 ms)

DISCUSSION AND CONCLUSION

Children differ from adults in many aspects. These differences are due to the large variability of body size, mass distribution, characteristics of the developing body structures, and injury tolerance levels (Huelke, 1998; Brun-Cassan et al., 1993). The first two problems can be solved simply with the GEBOD program (TNO, 1999), according to age, body height and/or body weight of the desired human model. However, limited knowledge is available for the characteristics of the developing body structures such as head, vertebra column and lower extremities of children. For the multi-body mathematical models, joints properties and contact stiffnesses of body segments are the essential input data.

The lateral flexion properties of neck, thoracic, lumbar, hip, knee and ankle joints were considered as the key issues for the dynamic responses of the child pedestrians involved in traffic accidents, because the majority of child victims are struck from side by vehicles. Based on the analysis of the behavior of the functional unit for the lumbar vertebrae (Fig. 3a) and the knee joints (Fig. 3b) under lateral flexion mode, the simplified joint model (Fig. 4) was developed to derive the scale

factors of lumbar vertebra and knee joints. It was inspired by the scaling process for neck responses (Mertz et al., 1989). Compared to the scaling methods applied to infants (Melvin, 1995) and child occupants (Irwin and Mertz, 1997), the influences of both the age-dependent characteristics of ligaments and the developing anatomic structures were accommodated in this model. The scale factors of neck joint flexion for 3 and 6 years old children were close to the results by Yoganandan et al. (2000). Within the scope of the current study, no other results were found about the scaling of thoracic, lumbar and knee joints. Thus the validity of this scaling method needs a further verification.

For the lateral contact stiffnesses of long bones, the three-point bending model (Fig. 5) was used to calculate the scale factors from adult data. Without geometric data for long bones, it was assumed that the outer diameter of long bones is proportional to the circumference of the corresponding body part. For example, the diameter of tibia bone is based on the circumference of lower leg. It was found that the contact stiffness of a long bone depends on the cross-section, length and the elastic modulus of the bone as well. The scale factors for the thorax and head were adopted from the studies of Hamilton et al. (1988) and Mertz et al. (1989), respectively.

Because no experiments of child pedestrians have been conducted with cadavers, one feasible way to evaluate the effectiveness of the scaled children models is to reconstruct real world accidents. To examine the overall performance of these scaled child pedestrian models, two real-world accidents were reconstructed in this study. Head responses from the mathematical simulations in both cases correlated well with the head injuries in accidents. Meanwhile, the injury parameters for other body segments were also consistent with the injury outcomes in accidents. The trajectories of the vehicles were compared with that recorded on the accident reports, as well as the throw-out distance of children. Generally the results of the accident reconstructions were acceptable.

There are still a number of limitations in the current study. First, the mechanical properties of child bones were limited. It was assumed that the elastic modulus of parietal bone in Fig. 2(a) could be applied to other body areas. This implies that the mechanical properties of bones in the whole body are same as the parietal bone or follows the same ratio between adults and children. Second, the scale factors of ligament properties were only obtained from the capsular and the anteromedial ligaments (Fig. 2b). Third, it was assumed that the width of tibia condyle (Fig. 4) is proportional to width of knee joint, whereas the length of medial collateral ligament is proportional to the length of lower leg. Similar assumptions was also applied to the neck, thoracic and lumbar vertebrae. Fourth, the mechanical properties of hip joint and the contact stiffness of pelvis area were not scaled from an anatomic point of view, because of the complexity of their structures. Unfortunately, those properties are important for the responses of child pedestrians, since the bumper and hood front edge may directly strike the pelvis and abdomen. Finally, it is insufficient to evaluate the validity of child pedestrian models with the data from two car-child pedestrian accidents. More well documented accidents are desirable. All of these problems affected the accurate evaluation of the performance of child pedestrian models.

Most of the uncertainties mentioned above are mainly due to the lack of biomechanical data of children. To improve reliability of current scaling methods, more complete experiment data for biological material are desirable. Understanding of the dynamic behavior of human body structures is also essential in order to properly build up the detailed mathematical models for various joints.

Despite the limitations in the current study, the results of accident reconstructions indicated the capability of the scaled models to predict the kinematic responses of child pedestrians under lateral impact loading. For the further development of child pedestrian mathematical models, the significance of joint properties and stiffness of body segments will be clarified by factorial analysis. Hip joint and pelvic stiffnesses will be scaled using the detailed description of anatomic structure. Moreover, an improved spinal column with separate vertebral disks should allow the proper simulation of the impact kinematics in the neck, thoracic and lumbar spine area.

ACKNOWLEDGEMENT

This study is sponsored by the Swedish National Road Administration (Vägverket).

REFERENCES

Ashton, S. J., Hayes, H. R. M. and Mackay, G. M. (1974) Child Pedestrian Injuries, *Proc. Int. Meeting on Biomechanics of Trauma in Children*, pp. 159-170.

Ashton, S. J. (1979) Some Factors Influencing the Injuries Sustained by Child Pedestrians Struck by the Fronts of Cars, *Proc. 23rd Stapp Car Crash Conf.*, SAE Paper 791016, pp. 351-380.

Beusenberg, M. C., Happee, R., Twisk, D. and Janssen, E. G. (1993) Status of Injury Biomechanics for the Development of Child Dummies, *Child Occupant Protection Symposium*, SP-986, SAE Paper 933104, pp. 219-241.

Brun-Cassan, F., Page, M. and Pincemaille, Y. (1993) Comparative Study of Restrained Child Dummies and Cadavers in Experimental Crashes, *Child Occupant Protection Symposium*, SP-986, SAE Paper 933105, pp.243-259.

Frank, H. N. (1987) Musculoskeletal System: Anatomy, Physiology and Metabolic Disorders, Volume I, Part II, The Ciba Collection of Medical Illustrations, USA.

Hamilton, M. N., Chen, H. F., Guenther, D. A. and Cheng, P. (1988) Computer Simulation of the Child Thorax, *Proc. 32nd Stapp Car Crash Conf.*, SAE Paper 881724, pp. 165-184.

Hubbard, R. P. and Soutas-Little, R. W. (1984) Mechanical Properties of Human Tendon and their Age Dependence, *Journal of Biomechanical Engineering*, Vol.106**,** pp. 144-150.

Huelke, D. F. (1998) An Overview of Anatomical Considerations of Infants and Children in the Adult World of Automobile Safety Design, *Proc. 42nd Annual Proceedings of Association for the Advancement of Automotive Medicine*, pp. 93-113.

Irwin, A. and Mertz, H. J. (1997) Biomechanical Basis for the CRABI and Hybrid III Child Dummies, *Proc. 26th Stapp Car Crash Conf.*, SAE Paper 973317, pp. 261-272.

Kapandji, I. A. (1970) The Physiology of the Joints. Volume Three. The Trunk and the Vertebral Column, Churchill Livingstone.

Kumaresan, S., Yoganandan, N. and Frank, A. P. (1997) Age-Specific Pediatric Cervical Spine Biomechanical Responses: Three-Dimensional Nonlinear Finite Element Models, *Proc. 41st Stapp Car Crash Conf.*, SAE Paper 973319, pp. 31-61.

Mcpherson, G. K. and Kriewall, T. J. (1978) The Elastic Modulus of Fetal Cranial bone: A First Step Towards and Understanding of the Biomechanics of Fetal Head Molding, *Journal of Biomechanics*, Vol.**13**(1), pp. 9-16.

Melvin, J. W. (1995) Injury Assessment Reference Values for the CRABI 6-month Infant Dummy in a Rear-Facing Infant Restraint with Airbag Deployment, *SAE International Congress and Exposition*, SAE Paper 950872, pp. 1-12.

Mertz, H. J. (1984) A Procedure for Normalizing Impact Response Data, *Proc. Government/Industry Meeting and Exposition*, SAE 840884, pp. 1-8.

Mertz, H. J., Irwin, A. L., Melvin, J. W., Stalnaker, R. L. and Beebe, M. S. (1989) Size, Weight and Biomechanical Impact Response Requirements for Adults Size Small Female and Large Male Dummies, *SAE International Congress and Exposition*, SP-782, SAE Paper 890756, pp.133-142.

Ohashi, H., Ono, K., Sasaki, A., Ohashi, N., Misawa, S. (1990) The Present Situation of Pedestrian Accidents in Japan, *Proc. Int. IRCOBI Conf. Biomechanics Impacts*, pp. 283-292.

Pitt, R., Guyer, B., Hsien, C. and Malek, M. (1990) The Severity of Pedestrian Injuries in Children: An Analysis of the Pedestrian Injury Causation Study, *Accident Analysis & Prevention*, Vol.**22**(6), pp. 549-559.

Sturtz, G., Suren, E. G., Gotzen, L., Behrens, S. and Richter, K. (1976) Biomechanics of Real Child Pedestrian Accidents, *Proc. 20th Stapp Car Crash Conf.*, SAE Paper 760814, pp. 467-510.

TNO (1999) MADYMO User's Manual 3D. Version 5.4, TNO Road-Vehicles Research Institute.

Wismans, J., Janssen, E. G., Koppens, W. P. and Lupker, H. A. (1994) Injury biomechanics (course textbook).

Yang, J. K. and Kajzer, J. (1992) Computer Simulation of Impact Response of the Human Knee Joint in Car-pedestrian Accidents, *Proc. 36th Stapp Car Crash Conf.*, SAE Paper 922525, pp. 203-217.

Yang, J. K. (1997) Injury Biomechanics in Car-Pedestrian Collisions: Development, Validation and Application of Human-Body Mathematical Models, Ph.D Dissertation, Chalmers University of Technology, Göteborg, Sweden.

Yang, J. K., Lövsund, P., Cavallero, C. and Bonnoit, J. (2000) A Human-Body 3D Mathematical Model for Simulation of Car-Pedestrian Impacts, *Journal of Crash Prevention and Injury Control*, Vol.**2**(2), pp. 131-149.

Yoganandan, N., Pintar, A. F., Kumaresan, S., Gennarelli, A. T., Sun, E., Kuppa, S., Maltese, M. and Eppinger, H. R. (2000) Pediatric and Small Female Neck Injury Scale Factors and Tolerance Based on Human Spine Biomechanical Characteristics, *Proc. Int. IRCOBI Conf. Biomechanics Impacts*, pp. 345-359.